Tellus (1982), *34*, 579–587

Small scale drainage front

By L. MAHRT, *Department of Atmospheric Sciences, Oregon State University, Corvallis, Oregon 97331 U.S.A.*, and SØREN LARSEN, *Meteorology Section, Risø National Laboratory, 4000 Roskilde, Denmark*

(Manuscript received August 4, 1981; in final form March 3, 1982)

ABSTRACT

A case study of nocturnal drainage flow is presented. The flow descends a gentle slope of a few percent extending about one half kilometer down to Roskilde Fjord in northeast Denmark. Opposing larger scale flow initially delays the advance of the drainage flow. After several hours delay, the drainage flow arrives at the coast as a sudden relatively deep surge of cold air.

This surge of cold air significantly disturbs the immediate overlying flow. Even though the surge of cold air is characterized by high Richardson number and weak turbulent activity, this drainage front induces low Richardson number and significant turbulent activity in the overlying flow resulting in an "upside down" structure to the "boundary layer". The drainage flow following the initial surge is thinner, weaker and nearly stationary except for occasional thicker pulses of cold air.

1. Introduction

Previous studies of drainage of cold air down sloped terrain have primarily addressed relatively strong flows over relatively steep slopes or slopes of large horizontal extent (e.g. Schwerdtfeger, 1970; Yoshino, 1975). Previous observations of slope flows rarely include turbulence properties.

The present study examines tower observations of cold-air drainage occurring at Risø, Denmark (55°42′N, 12°5′E) on the evening of October 17–18, 1978. The slope at Risø (Fig. 1) is approximately 4% occurring on a scale of about one half kilometer which is rather typical of undulating terrain covering much of the land surface of the world. Throughout most of the night, the slope flow is one or two meters per second over a depth of several meters.

On this evening, synoptic stations in eastern Denmark reported clear skies and normally weak southwesterly surface flow which would act to oppose drainage flow at Risø. The present study will show that drainage flows occurring over such small slopes may overcome an adverse synoptic flow and exhibit some features (in scaled down version) which are least superficially similar to more violent katabatic outbreaks observed over larger scale and steeper slopes (e.g. Streton, 1963).

2. Observational site and instrumentation

The measurements were obtained at the Risø National Laboratory in Denmark. The site is located on the east shore of Roskilde Fjord on the island Zeeland. For the data described here, the main region of interest is the southern part of the map in Fig. 1 where cold surface air flows westard down the slope toward the small 7 m mast (point B) located at the bottom of the slope. Further inland, east of the coastal slope, the terrain gently undulates between 10 and 30 meters. It is not known if the cold-air drainage originates entirely on the slope or if some of the cold air originated inland and spilled over the low ridge at the eastern edge of Fig. 1. More information on the nearby terrain and the observational site is presented in Gryning and Lyck (1980).

At the small mast, 10-minute averaged values of wind speed and instantaneous values of wind

0040-2826/82/060579-09$02.50/0

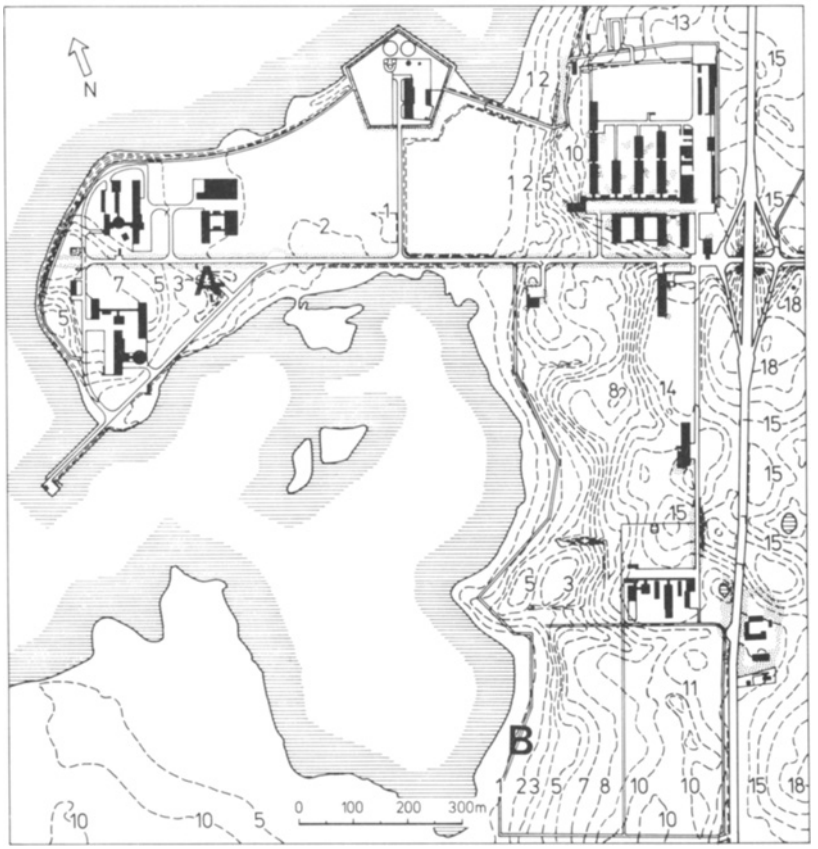

Fig. 1. Terrain contours (m) for the Risø area showing the 117 m tower (A) and the 7 m mast (B).

Table 1. *Specifications of accuracy and resolution of the instruments. The dynamic response of cup-anemometers and wind-vanes are best described by a distance constant. The wind-vane at the 7 m mast is artificially damped by viscous oil in the bearings. The accuracy and resolution estimates correspond to laboratory calibration conditions. For the present data overspeeding of the cup anemometers and radiation errors on the temperature measurements are of no importance. Here, u is the horizontal wind speed*

Measuring station	Instrument	Zero threshold ($m\ s^{-1}$)	Response time (s)	Accuracy better than	Resolution
117 m tower	Cup anemom.	0.25	1.5 m/u ($m\ s^{-1}$)	$\pm$ 5 cm s^{-1}	$\pm$ 5 cm s^{-1}
	Wind vane	0.30	0.25 m/u ($m\ s^{-1}$)	$\pm$ 1 °C	$\pm$ 1 °C
	thermometer	—	10 s	$\pm$ 0.02 °C	$\pm$ 0.1 °C
7 m mast	Cup anemom.	0.25	1.50 m/u	$\pm$ 5 cm	$\pm$ 5 cm
	Wind vane	0.30	20 m/u	$\pm$ 5 °C	$\pm$ 1 °C
	thermometer	—	10 s	$\pm$ 0.1 °C	$\pm$ 0.1 °C

direction and temperature were each recorded every 10 minutes at two different levels using an automatic data logger. The instrument response characteristics are listed in Table 1.

The drainage flow is also observed at the 117 m Risø Meteorology Tower (point A in Fig. 1) which is located on a low peninsula about one half kilometer downstream from the bottom of the slope and about

Table 2. *Data for the 117 m tower and small mast. Time refers to the middle of 10-minute averaging periods. Five minutes must be added to the times for the small mast*

	Downslope wind component (m s^{-1})						Potential temperature (K)							Standard deviation of lateral wind fluctuation (m s^{-1})		
	Small mast		117 m tower				Small mast		117 m tower					117 m tower		
Time	1.5 m	6.3 m	11 m	43 m	76 m	117 m	1.5 m	5.8 m	2 m	11 m	27 m	76 m	117 m	11 m	43 m	76 m
1940	0.61	1.43	1.35	2.74	4.24	4.63	278.8	280.0	280.12	280.61	280.97	282.36	282.67	0.18	0.14	0.21
1950	0.79	1.32	1.78	2.72	3.45	4.64	278.6	279.8	280.22	280.81	281.07	281.66	282.57	0.29	0.16	0.13
2000	0.14	0.11	1.43	2.13	3.14	4.63	278.2	279.5	280.42	280.81	281.07	281.66	282.67	0.24	0.13	0.20
2010	−0.14	0.19	1.12	1.90	3.32	4.64	277.8	278.7	280.22	280.81	280.97	281.96	282.67	0.17	0.11	0.11
2020	−0.66	0	1.06	2.09	4.02	4.71	277.9	278.7	280.12	280.71	280.97	282.26	282.57	0.09	0.11	0.04
2030	−0.33	1.36	1.07	2.19	4.19	5.08	277.5	278.9	280.02	280.61	280.87	281.96	282.57	0.12	0.12	0.09
2040	−1.24	−1.22	0.54	1.50	3.15	5.19	277.8	278.7	279.72	280.41	280.67	281.46	282.37	0.12	0.15	0.16
2050	−1.98	−2.13	−0.63	0.34	1.34	3.65	277.9	279.1	278.72	279.81	280.27	280.86	281.57	0.21	0.23	0.25
2100	−1.79	−1.58	−0.97	−0.09	1.14	3.85	277.6	279.1	278.12	279.41	280.07	280.66	281.57	0.11	0.19	0.34
2110	−1.69	−1.80	−0.71	−0.10	2.05	4.60	277.2	279.0	278.02	279.51	280.07	280.76	281.67	0.14	0.12	0.38
2120	−1.58	−0.75	−0.44	−0.17	1.90	4.59	277.9	279.4	278.52	279.31	279.97	280.56	281.57	0.14	0.21	0.45
2130	−0.29	−0.16	−0.44	0.69	2.28	4.43	277.1	278.9	278.32	279.81	280.17	280.86	281.77	0.09	0.26	0.36
2140	−0.50	−0.18	0.08	1.29	2.74	5.29	276.5	277.9	279.02	279.91	280.27	281.16	282.27	0.03	0.25	0.30
2150	−1.32	−0.66	0.37	1.10	2.44	4.79	276.5	278.4	279.32	280.11	280.37	281.06	282.07	0.08	0.20	0.28
2200	−1.47	−0.76	0.90	1.82	2.92	4.60	276.3	278.4	279.02	280.21	280.37	280.96	281.97	0.17	0.23	0.22
2210	−1.12	−0.32	0.76	1.94	3.12	4.70	276.5	278.2	278.82	280.01	280.37	281.06	282.07	0.23	0.17	0.18
2220	−1.55	−1.08	0.94	2.07	3.72	4.19	276.8	278.7	279.32	280.11	280.37	281.46	282.47	0.15	0.18	0.15
2230	−1.78	−1.00	0.43	1.78	3.67	3.85	276.1	278.6	279.02	279.81	280.17	281.96	282.67	0.27	0.26	0.16
2240	−1.53	−1.20	−0.31	1.29	3.25	4.20	276.1	278.4	278.62	279.61	279.87	281.16	282.47	0.11	0.29	0.28
2250	−1.61	−1.28	−0.17	1.89	4.05	3.89	276.0	278.4	278.42	279.21	279.87	281.96	282.57	0.09	0.17	0.20
2300	−1.53	−1.17	−0.16	1.58	3.64	3.67	276.0	278.3	278.22	278.91	279.57	281.76	282.57	0.09	0.12	0.13
2310	−1.65	−1.28	0	1.59	3.44	3.56	275.8	278.4	278.02	279.01	279.87	281.56	282.57	0.06	0.14	0.13
2320	−1.58	−0.96	−0.25	0.92	3.26	3.37	275.7	278.4	278.02	278.71	279.97	281.56	282.57	0.09	0.14	0.07
2330	−1.26	−0.94	−0.09	1.41	3.44	3.18	275.7	277.7	277.82	278.61	279.77	281.76	282.57	0.06	0.08	0.04
2340	−1.49	−0.37	−0.04	1.56	3.47	2.98	275.7	278.0	278.02	278.61	279.87	282.06	282.57	0.06	0.08	0.07
2350	−0.58	−1.04	0.24	2.33	3.80	3.05	274.9	277.6	277.82	278.91	280.07	282.36	282.77	0.06	0.05	0.07
0000	−0.45	0.12	0.72	2.52	4.10	3.24	275.8	277.8	277.72	279.31	279.97	282.26	282.67	0.12	0.05	0.05
0010	−0.63	−0.18	0.91	2.48	4.30	3.73	276.0	277.9	278.22	279.71	280.07	282.06	282.67	0.13	0.15	0.12

800 m north of the small mast. Since the flow in this study is essentially down the slope, the same air parcel does not pass both towers. At the 117 m tower, 10-minute averages of wind speed, wind direction, temperature and wind-direction variance are recorded every 10 minutes at several levels. The wind-direction variance pertains to the frequency band 1.2×10^{-3}–5 Hz and is further limited by a distance constant of approximately 0.25 m. The wind-direction variance is approximately equal to the variance of lateral wind fluctuations as long as the root mean square of the wind fluctuations remains small compared to the mean wind speed (see Appendix). For additonal descriptions of the instrumentation on the Risø tower see Table 1 and Kristinsen and Panofsky (1976). Data collected from the small mast and 117 m tower used in the present study are listed in Table 2.

Layer Richardson numbers at the 117 m tower were calculated using the temperature gradient and square of the magnitude of the vector shear for the layers 11–27 m, 27–76 m and 76–117 m. A surface Richardson number for the small mast is computed for temperatures at 1.5 m and 5.8 m and wind speed at 6.3 m.

3. Initial surge

Although the small mast and tower are separated in distance, and the tower is located on a rise about 5 m above the slope bottom, compositing the data

from both of the small mast and 117 m tower produces a self-consistent picture of airflow (Fig. 2). About 2000 L, a thin weak downslope flow of a few tens of cm s^{-1} and a few meters deep (Fig. 2) arrives at the small mast at the bottom of the slope. This arrival is accompanied by a temperature decrease of about 1 °C (Table 2). This weak drainage flow is not observed at the 117 m tower which is downstream from the slope bottom and contains no wind observations below 11 m.

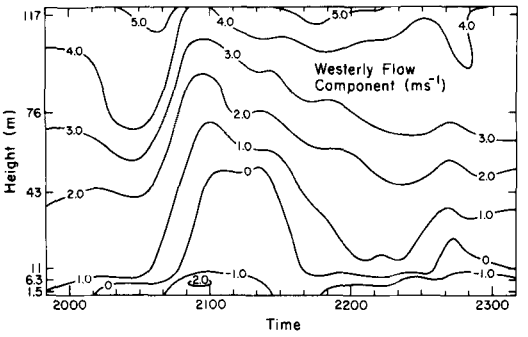

Fig. 2. Westerly flow component (m s^{-1}) as a function of height (m) and local time, composited from both the small mast 1.5 m and 6.3 m observational levels and the 117 m tower 11 m, 27 m, 43 m, 76 m and 117 m observation levels.

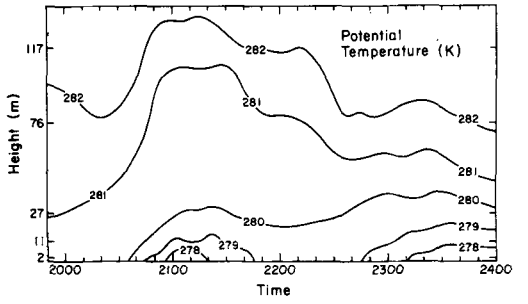

Fig. 3. Potential temperature (K) as a function of height (m) and local time at the 117 m tower (2 m, 11 m, 27 m, 76 m and 117 m observational levels).

Just prior to 2100 L, the downslope flow observed at the slope bottom is suddenly thicker and faster. This thick surge or drainage front arrives at the 117 m tower minutes later. The sudden onset or intensification of drainage flows has been reported previously in a number of studies summarized in Geiger (1975), Schwerdtfeger (1970) and recently reported in Abe (1979).

The arrival of the cold-air surge at the downstream tower leads to significant temperature drops throughout the 117 m tower layer (Fig. 3). The depth of the actual cold-air surge appears to be a few tens of meters deep while the cooling above the surge appears to be due to adiabatic cooling associated with the surge pressure field and resulting convergence, as is discussed later in this section. The cold-air bulge at the 117 m tower is characterized by large-layer Richardson number (Fig. 4) and only minor turbulent activity but induces increased shear, low Richardson number and substantial turbulent activity in the overlying westerly flow. While the correlation between the lateral wind fluctuations and the Richardson number is not perfect (Fig. 4), the relationship seems sufficiently strong to identify the region above the surge as a location of significant turbulent activity. The same "upside-down" structure to the "boundary layer" occurs again during a secondary surge of cold air beginning around 2230.

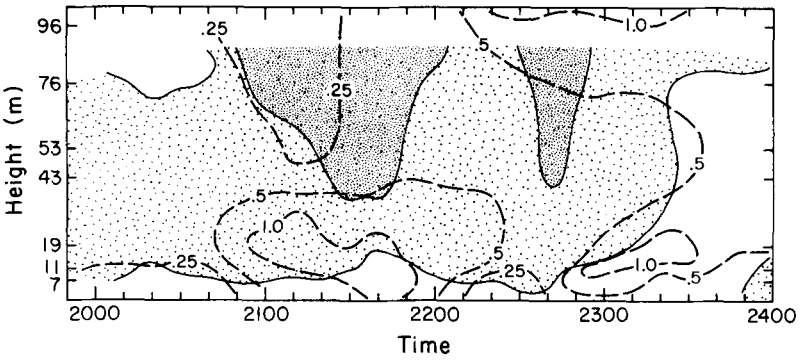

Fig. 4. Standard deviation of lateral wind fluctuation (m/s) measured at 11 m, 43 m and 76 m levels at the 117 m tower; dark shading indicates values > 0.25 m s^{-1} and light shading > 0.1 m s^{-1}. Isolines of layer-Richardson number (dashed lines) are also shown.

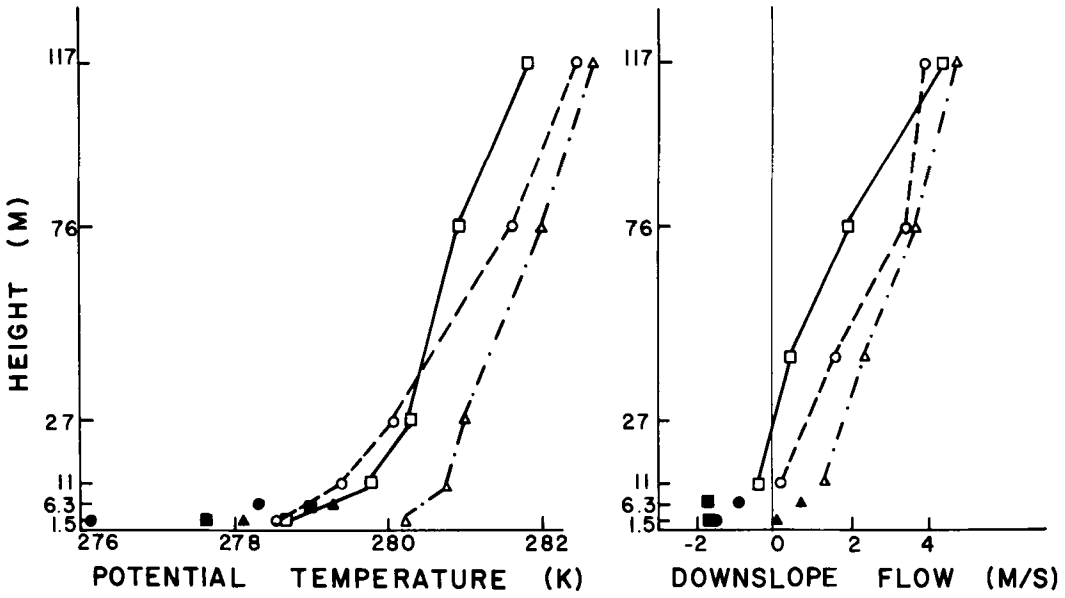

Fig. 5. Averaged values of potential temperature and downslope flow before the drainage surge 1940 L–2030 L (triangles) during the surge 2040 L–2110 L (squares) and after the surge 2150–2340 (circles). Closed symbols refer to corresponding values for the small mast.

A thick head developing at the leading edge of gravity currents has been observed in several laboratory studies (e.g. Bitter and Simpson, 1978). The continuous stratification and height-dependent ambient wind of the present situation precludes definite association of these events with laboratory phenomena or hydraulic jump-like conditions.

The bulge of cold easterly flow survives about one hour. It is not known if the drainage front stalled over the water near the coast or had extended out over the fjord and was eliminated by heat flux from the warmer water. Photographs of steam fog over a nearby fjord (not shown) suggest that drainage flows may extend several hundred meters over the water terminating at a sharp front.

The opposing westerly flow seems to decelerate significantly as it rises up over the cold air bulge (Figs. 2, 5). The westerly momentum decreases over a layer which appears to be much thicker than the drainage flow. Therefore turbulent mixing is ruled out as a primary explanation even though the air above the cold-air drainage is characterized by low Richardson number and large velocity variance. Probably the deceleration is associated with a pressure disturbance. A positive pressure perturbation advancing with and above the cold-air bulge could explain the observed deceleration of the westerly flow over a deep layer. Decreasing westerly momentum above the bulge can result directly from the opposing horizontal gradient of the perturbation pressure and indirectly from upward vertical advection of weaker westerly momentum. This vertical advection is caused by convergence and rising motion induced by the pressure field at the drainage front.

Rapid cooling over a depth much greater than the drainage (Figs. 3, 5) also precludes turbulent mixing as the main influence on the temperature field. The time scale is too short for significant radiative flux divergence and it is unlikely that sharp temperature drops coinciding with the surge event would be produced by horizontal advection in the westerly flow.

The remaining and most likely explanation is adiabatic cooling associated with rising motion as the westerly flow is forced to rise up over the bulging and advancing easterly cold air. The observed cooling could be explained by a vertical displacement of about 40 m, comparable to the depth of the bulge of downslope flow. This vertical displacement could also explain most of the observed deceleration of the westerly flow although direct deceleration by the perturbation pressure field can not be ruled out. The fact that the

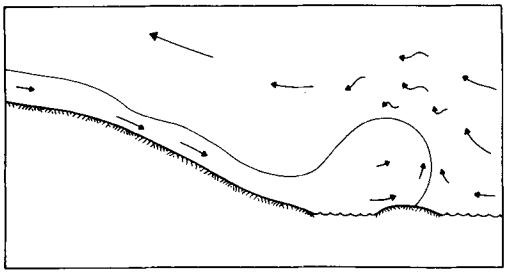

Fig. 6. Schematic depiction of downslope flow and frontal surge based on observations from the 117 m tower and small mast.

deceleration becomes small above roughly 100 m where the shear becomes small, while significant cooling continues to higher elevations is consistant with expected influences of vertical advection. The results of Figs. 2–5 are schematically composited into a plausible flow picture shown in Fig. 6.

4. Surge dynamics

The fact that a sudden pulse of particularly thick cold air is not observed until approximately six hours after radiational sunset suggests that the drainage of cold air toward the coast is initially prevented by the opposing synoptic flow. The abrupt termination of the slope and low coastal bluff may also contribute to the local thickening of the initial cold-air surge at the 117 m tower.

The likelihood of advance of the cold-air drainage can be posed in terms of a scale analysis of the equation for momentum in the downslope direction (Ball, 1956) which can be written in the form

$$\frac{du}{dt} = g\frac{\theta}{\theta_0}S - g\frac{\bar{\theta}}{\theta_0}\frac{\partial}{\partial x}h - g\frac{h}{\theta_0}\frac{\partial}{\partial x}\bar{\theta}' - \frac{1}{\rho}\frac{\partial p}{\partial x} - \frac{\partial \overline{u'w'}}{\partial z} \tag{1}$$

u is the flow component in the downslope direction x, t is time, θ is the potential temperature deficit of the flow, with a value of about 2 K, $\bar{\theta}$ is the vertical average of the potential temperature deficit between level z and h, the top of the drainage flow (order of 10 m), θ_0 is a basic state potential temperature and S is the terrain slope approximately equal to 3.7%. p is the pressure perturbation largely associated with the advance of the drainage flow but also influenced by three-dimensional topographical effects. $\overline{u'w'}$ is the turbulent flux of downslope momentum in the z-direction (perpendicular to the slope). Coriolis effects do not significantly influence the local slope flow since it has a Lagrangian time scale of less than one hour. For this reason the surface flow direction is approximately aligned with the slope vector.

The slope flow is driven by the buoyancy acceleration $g(\theta/\theta_0)S$, which is about 2.6×10^{-3} m s^{-2} using the above parameter values. The drainage flow is also influenced by a thermal wind term due to the varying depth of the drainage flow which scales like

$$\left| g\frac{\theta}{\theta_0}\frac{\partial}{\partial x}h \right| \sim g\frac{\theta}{\theta_0}\frac{h}{L} = g\frac{\theta}{\theta_0}S\frac{h}{\Delta z} \tag{2}$$

where Δz is the surface elevation drop over the horizontal length scale L. Since $h/\Delta z$ is of the order of one, this term should be of the same order of magnitude as the buoyancy term, although its importance is probably concentrated near the drainage front where $\partial h/\partial x$ is large. If horizontal temperature gradients scale like θ/L, then the scale value of the thermal wind term due to temperature gradients along the slope is

$$\left| \frac{gh}{\theta_0}\frac{\partial}{\partial x}\bar{\theta} \right| \sim g\frac{\theta}{\theta_0}\frac{h}{L} \tag{3}$$

and is therefore the same order of magnitude as that in (2). The scale analysis (2–3) assumes that the source of the cold air is at the top of the low coastal ridge (right-hand side of Fig. 1) and not further inland. These latter two terms (2–3) can drive cold air from the interior toward the fjord even without a slope effect.

Positive perturbation pressure at the drainage front acts to decelerate the drainage flow and leads to complete horizontal deceleration of the opposing ambient flow at the surface. Estimating the perturbation pressure gradient in terms of the ambient flow deceleration we obtain

$$\frac{1}{\rho_0}\frac{p}{L_p} \sim \frac{U^2}{L_p} \tag{4}$$

where U is the ambient flow and L_p is the horizontal length scale of the pressure disturbance of unknown value. Although the magnitude of this

term cannot be estimated, its importance is strongly suggested by the analysis of Section 3. The synoptic scale pressure gradient acceleration appears to be about 10^{-3} m s^{-2} and is therefore probably of direct importance.

The turbulent momentum flux $\overline{u'w'}$ is associated with surface drag and mixing between the slope flow and overlying fluid. As in the slope flow studied by Manins and Sawford (1979), the surface drag is estimated to be unimportant particularly since the drainage flow here is only weakly turbulent. Even if turbulent, the flux divergence in the drainage flow would be only of the order of 10^{-4} m s^{-2} for a speed of 2 m s^{-1} and depth of 40 m (or, behind the bulge, a speed of 1 m s^{-1} and depth of 10 m). These estimates used a drag coefficient of 10^{-3}, typical of very stable boundary layers.

Mixing between the upstream slope flow and overlying opposing flow could also delay the arrival of the drainage flow at the coast. However, this mixing probably does not significantly influence the interior of the cold-air near the surface which is only weakly turbulent. Since the flow above the drainage flow is more turbulent, it would not be very useful to adopt the usual parameterization of such momentum exchange in terms of downward entrainment as in Ellison and Turner (1959) and others. It may be more useful to think of the gravity flow losing fluid to the overlying turbulent transition layer as in Bitter and Simpson (1978).

The above parameters which are thought to be most important can be combined into the following slope Richardson number

$$R_s \equiv \frac{g\frac{\theta}{\theta_0} hS}{U^2} \tag{5}$$

where again U is the speed of the opposing flow with a typical 10 m value of 1.1 m s^{-1} prior to the onset of the drainage flow. This slope Richardson number is of the same form but of different physical interpretation than the slope Richardson number analyzed in Brost and Wyngaard (1978) and Lenschow *et al.* (1979). In particular, drainage flow is most likely to advance when the above Richardson number is large which will occur when the buoyancy acceleration $g(\theta/\theta_0)S$ is large or the opposing ambient flow is weak.

In the present flow case, the slope Richardson number increases with time due to increasing temperature deficit and presumed increasing depth of the cold air inland. This number also increases due to slowly decreasing onshore ambient flow. The weakening of the westerly onshore flow may be due to synoptic scale trends or increasing land-sea temperature contrast.

Just prior to the arrival of the cold-air drainage at the coast, the value of the slope Richardson number had increased by several factors to a value of approximately

$$R_s \simeq \frac{10 \text{ m s}^{-2} (2 \text{ K}/280 \text{ K}) \, 10 \text{ m } 3.7 \times 10^{-2}}{(1.1 \text{ m s}^{-1})^2}$$
$$\simeq 2.2 \times 10^{-2}$$

This value should be considered to be very rough since the estimation of the depth and average temperature deficit of the gravity flow and choice of level of the opposing wind speed are somewhat subjective. While the slope Richardson number should be a useful indicator of the probability of the advance of a gravity flow, this number does not consider the influence of the thermal wind term

$$g\frac{\theta}{\theta_0}\frac{\partial}{\partial x}h.$$

For comparison, consider the limiting case where the slope-buoyancy term is unimportant and the flow advances primarily through the termal wind term due to build-up of cold air inland. Then the relevant parameter is simply the bulk Richardson number,

$$R_b = \frac{g}{\theta_0}\bar{\bar{\theta}}h/U^2 \tag{6}$$

which attains a value of roughly 0.7 prior to the cold-air advance. This value is probably fortuitously close to the value predicted by Benjamin (1968) (see also Turner, 1973, p. 73) for steady state advance of a layer of dense fluid within a lighter fluid. In their studies, U is the steady state advance speed corresponding to a balance between the hydrostatic pressure gradient, analogous to

$$g\frac{\bar{\bar{\theta}}}{\theta_0}\frac{\partial}{\partial x}h,$$

and the opposing gradient of perturbation or dynamic pressure proportional to U^2. This dynamic pressure gradient acceleration is analogous to (4) if we choose $L_p = L$.

The value of $R_B = 0.7$ for the present case is two

or three factors smaller than values computed by Simpson (1969) for several atmospheric cases of sea breeze events and related phenomena. The greater relative flow speed and lower Richardson number in the present case could reflect acceleration due to the slope effect or may be due to differences in the definition and calculation of the temperature deficit and velocity and depth scales.

In summary, the advance of the gravity flow should be determined primarily by the slope Richardson number if the thermal wind term (3) is small compared to the slope-buoyancy term (2), that is if $h/\Delta z$ is small compared to one. Otherwise, the value of the bulk Richardson number must also be considered.

5. Quasi-stationary stage

The bulge of cold easterly flow at the 117 m tower yields to warmer westerly flow at all observational levels after about one hour (Figs. 2–3, 5). After this period, the drainage flow does not normally reach the 117 m tower or at least is confined to levels below the lowest wind observations at 11 m, except for a number of weak pulses of easterly cold air which engulf the 11 m observational level. The largest of these weak pulses occurs about 2 hours after the main initial surge. Pulses of cold-air drainage have been previously reported by a number of studies referenced in Geiger (1975) and recently reported by Doran and Horst (1981). Aichele (1953) has attributed pulsation of cold-air drainage to restriction of the current by a terrain constriction. Here the initial main surge and subsequent weak pulse apparently form due to the build-up of cold air forced by the opposing larger scale flow and/or the variation in the opposing flow with time.

6. Conclusions

Relatively weak small-scale slopes can induce sufficient nocturnal cold-air drainage to overcome opposing large-scale flow. Here the drainage flow overcomes opposing flow when the slope Richardson number has increased to about 2×10^{-2} corresponding to a bulk Richardson number of about 0.7. Then cold-air drainage advances as a thick frontal bulge.

This frontal surge of cold air is characterized by large layer Richardson number and weak turbulence. However, the front induces significant deceleration and fluctuations in the overlying flow which is forced upward over the cold-air bulge. After the initial frontal surge, the downslope flow is weaker, thinner and nearly stationary except for a few thicker pulses.

Surface heating over the warmer water of the narrow fjord may have helped maintain the slope flow throughout the night. In contrast, Heywood (1933) found katabatic flows down valley slopes to frequently terminate after a few hours apparently due to filling up the valley with cold air.

Examination of a number of other drainage flows at Risø indicates that a well-defined initial surge of drainage flow seems to occur only with opposing larger scale flow. Otherwise the drainage flow normally develops earlier in the evening and more gradually. The above observations as well as those on more extensive slopes suggest that mesoscale fronts, in general, are generated in the presence of some opposing larger scale flow and may induce significant disturbances well above the frontal convergence zone.

7. Acknowledgements

The assistance of S. E. Gryning and helpful comments of the reviewers are appreciated. This material is based upon work supported by the Meteorology Program of the National Science Foundation under Grant No. ATM-7908308 and the Risø National Laboratory, Denmark.

8. Appendix

The wind direction fluctuation D', for a mean flow $\bar{u}$, can be written as

$$D' \equiv \operatorname{atan}\left(\frac{v'}{\bar{u} + u'}\right)$$

For the usual atmospheric case $u' \ll \bar{u}$,

$$D' \simeq \operatorname{atan}\left[\frac{v'}{\bar{u}}(1 - u'/\bar{u})\right]$$

For the case where direction fluctuations are small

$$\overline{D'^2} \simeq \frac{1}{\bar{u}^2}\left[\overline{v'^2} - \frac{\overline{2u'v'^2}}{\bar{u}} + \frac{\overline{v'^2u'^2}}{\bar{u}^2}\right]$$

Again using the condition $u' \ll \bar{u}$, we obtain

$$\overline{D'^2} \simeq \frac{\overline{v'^2}}{\bar{u}^2}$$

REFERENCES

Abe, T. 1979. Periodic abrupt changes of wind observed at Syowa Station, Antarctica. *Tenki. 26*, 688–692.

Aichele, H. 1953. Kaltluftpulsationen. *Met. Rundsch. 6*, 53–54.

Ball, F. K. 1956. The theory of strong katabatic winds. *Aust. J. Phys. 9*, 373–386.

Benjamin, T. B. 1968. Gravity currents and related phenomena. *J. Fluid Mech. 31*(2), 209–248.

Bitter, R. E. and Simpson, J. E. 1978. Experiments on the dynamics of a gravity current lead. *J. Fluid Mech. 88*, Part 2, 223–240.

Brost, R. A. and Wyngaard, J. C. 1978. A model study of the stably stratified planetary boundary layer. *J. Atmos. Sci. 35*, 1427–1440.

Doran, J. C. and Horst, T. W. 1981. Velocity and temperature oscillations in drainage winds. *J. Appl. Meteorol. 20*, 361–364.

Ellison, T. H. and Turner, J. S. 1959. Turbulent entrainment in stratified flows. *J. Fluid Mech. 6*, 423–448.

Geiger, R. 1975. *The climate near the ground.* Harvard University Press, 611 pp.

Gryning, S. and Lyck, E. 1980. Medium-range dispersion experiments downwind from a shoreline in near-neutral conditions. *Atmos. Environ. 14*, 923–931.

Heywood, G. S. P. 1933. Katabatic winds in a valley. *Quart. J. Roy. Meteorol. Soc. 59*, 47–58.

Kristinsen, L. and Panofsky, H. A. 1976. Climatology of wind direction fluctuations at Risø. *J. Appl. Meteorol. 15*, 1279–1283.

Lenschow, D. H., Stankov, B. and Mahrt, L. 1979. The rapid morning boundary layer transition. *J. Atmos. Sci. 36*, 2108–2124.

Manins, P. C. and Sawford, B. L. 1979. Katabatic winds: a field case study. *Quart. J. Roy. Meteorol. Soc. 105*, 1011–1025.

Schwerdtfeger, W. 1970. *The climate of the Antarctic.* World Survey of Climatology 14, 253–355. (ed. H. E. Landsberg), Amsterdam: Elsevier Publishing Co.

Simpson, J. E. 1969. A comparison between laboratory and atmospheric density currents. *Quart. J. Roy. Meteorol. Soc. 95*, 758–765.

Streton, N. A. 1963. Some observations of Antarctic katabatic winds. *Aust. Met. Mag. 42*, 1–23.

Turner, J. S. 1973. *Buoyancy effects in fluids.* Cambridge University Press, 367 pp.

Yoshino, M. 1975. *Climate in a small area.* University of Tokyo Press, 549 pp.